ROYAL SOCIETY OPEN SCIENCE

Research

Check for updates

Authors for correspondence:
M. E. Ries
e-mail: m.e.ries@leeds.ac.uk
A. Radjenovic
e-mail: aleksandra.radjenovic@glasgow.ac.uk

[†]Present address: Advanced Engineering Materials Group, School of Chemical and Process Engineering, University of Leeds, Leeds LS2 9JT, UK.
[‡]Present address: Institute of Cardiovascular and Medical Sciences, BHF Glasgow Cardiovascular Research Centre, University of Glasgow, Glasgow, UK.

THE ROYAL SOCIETY PUBLISHING

Imaging of nuclear magnetic resonance spin–lattice relaxation activation energy in cartilage

R. J. Foster[1,4,†], R. A. Damion[1], M. E. Ries[1], S. W. Smye[3,4], D. G. McGonagle[2,4], D. A. Binks[2,4] and A. Radjenovic[2,4,‡]

[1]Soft Matter Physics Group, School of Physics and Astronomy, [2]Leeds Institute of Rheumatic and Musculoskeletal Medicine, and [3]School of Medicine, University of Leeds, Leeds LS2 9JT, UK
[4]Leeds Musculoskeletal Biomedical Research Unit, Chapel Allerton Hospital, University of Leeds, Leeds LS4 7SA, UK

RJF, 0000-0002-5337-3615

Samples of human and bovine cartilage have been examined using magnetic resonance imaging to determine the proton nuclear magnetic resonance spin–lattice relaxation time, T_1, as a function of depth within the cartilage tissue. T_1 was measured at five to seven temperatures between 8 and 38°C. From this, it is shown that the T_1 relaxation time is well described by Arrhenius-type behaviour and the activation energy of the relaxation process is quantified. The activation energy within the cartilage is approximately $11 \pm 2 \, \text{kJ mol}^{-1}$ with this notably being less than that for both pure water ($16.6 \pm 0.4 \, \text{kJ mol}^{-1}$) and the phosphate-buffered solution in which the cartilage was immersed ($14.7 \pm 1.0 \, \text{kJ mol}^{-1}$). It is shown that this activation energy increases as a function of depth in the cartilage. It is known that cartilage composition varies with depth, and hence, these results have been interpreted in terms of the structure within the cartilage tissue and the association of the water with the macromolecular constituents of the cartilage.

1. Introduction

Articular cartilage is mainly composed of type II collagen, glycosaminoglycans (GAGs) and interstitial water. The distribution of these constituents is heterogeneous and the collagen is

also anisotropic. The organization and complex interplay of these components imbues the tissue with beneficial load-bearing and lubrication properties and, because of this, cartilage and its function have been the subject of recent intense research, for example see the reviews in Binks et al. [1], Mow & Huiskes [2], Vaca-González et al. [3] and Wilson et al. [4] and the mini-review series introduced by Pacifici [5] on cartilage biology and pathology. A major motivating factor for the study of articular cartilage is that cartilage is a key site for both the initiation and progression of osteoarthritis (OA), which is a highly prevalent age-related condition for which the treatment for the end stage of the disease is joint replacement [6]. The early stages of OA are associated with changes in the macromolecular composition of the cartilage and softening of the tissue due to increased water content, which is thought to occur prior to tissue loss.

Owing to its non-invasive nature, magnetic resonance imaging (MRI) is an extremely powerful tool for the study of cartilage tissue, as it can probe the properties of the water within the tissue body. Through understanding the interaction of the interstitial water with the macromolecular constituents within the cartilage tissue and the effect of this on MRI relaxation times, indirect information on the extracellular matrix can be determined. The challenge is then to link this information on the structure and composition of the tissue to its biochemical and biomechanical properties.

Quantitative MRI has been used to study cartilage, both *in vitro* [7–10] and *in vivo* [11–14]. Measurements of the spin–spin relaxation time, T_2, have been shown to be sensitive to a wide range of different parameters including collagen concentration [15], fibril orientation [10], fibril organization [16], GAGs [17] and changes in tissue water content [18]. Quantitative mapping of more complex MRI parameters, such as the relaxation time in the rotating reference frame [19,20], relaxation times of sodium nuclei [21–23] and gagCEST [24,25], have also been reported to be sensitive to changes in GAG content within the tissue.

Measurement of the spin–lattice relaxation time, T_1, has often been disregarded because it shows relatively little contrast or variation throughout the cartilage body [26]. T_1 typically exhibits a monotonic decrease through the depth of the cartilage [27]. In addition, long measurement times for T_1 have meant that investigators interested in clinical applications have instead focused on imaging T_1 in the presence of a gadolinium contrast agent, based on the dGEMRIC method [28], because it has been shown that the contrast agent tends to concentrate in regions of lowest GAG content and can therefore be used to show regions of early cartilage degeneration, before the formation of focal lesions [13,29].

However, it has also been shown that T_1 is sensitive to the changes in water content [17,27,30], and therefore, it offers the opportunity to use the interstitial water within cartilage as a probe to study the structure and composition of the cartilage. In the early stages of OA, it has been reported that the water content of cartilage increases because the degeneration disrupts the extracellular matrix. It has therefore been postulated that the measurement of water content can provide useful information on the degree of early cartilage degeneration, and thus, T_1 could provide an effective biomarker in cartilage [27].

The Arrhenius activation energy, E_A, is a widely used experimentally determined parameter that relates the rate of a physical or chemical process to temperature. Within the context of NMR relaxation times, this can be interpreted as an energy barrier for the relaxation process to occur. Spin–lattice relaxation in biological samples results predominantly from dipolar interactions between the hydrogen nuclei in water molecules and the interactions of these nuclei with the surrounding constituent macromolecules. The strength of these interactions is determined, in part, by the rotational and translational motion of the water molecules. The temperature dependence of this motion gives rise to the temperature dependence of the relaxation time, T_1 [31]. Activation energies have also been determined in diffusion NMR in *ex vivo* white matter [32] and in muscle tissue [33]. This approach has been used within clinical MRI to monitor tissue temperature in MR thermometry [31,34].

T_2 has also been shown to be sensitive to water content, and an increase in T_2 relaxation time with increasing temperature has been observed. However, in tissues, T_2 values are affected by a wide variety of different factors such as slow molecular tumbling and chemical exchange, resulting in $T_2 \ll T_1$ [21], and these factors complicate the temperature dependence [31]. Indeed, the analysis of proton spin–spin relaxation temperature dependence in muscle tissue resulted in an activation energy that was negative [33].

In this study, we have therefore chosen to investigate the depth-wise change in T_1 relaxation time as a function of temperature to extract the depth dependence of the E_A for the T_1 relaxation process, in order to determine if new structural information could be highlighted by this approach. We present activation energy profiles for the first time in articular cartilage and suggest a possible explanation for our observations.

2. Material and methods

2.1. Cartilage samples

Samples of human and bovine cartilage were examined *in vitro* using MRI. Human cartilage from the tibial plateau was obtained post-mortem through the Leeds GIFT2 Research Tissue Project [35] in accordance with ethical approval 10/H1313/48 from the Local Research Ethics Committee (Leeds). Informed consent was obtained from donors' next of kin by NHS Blood and Transplant Tissue Services on behalf of GIFT2, under a Service Level Agreement to their agreed policies and procedures which are NHS Research Ethics Committee approved. This is in line with approved standards for taking consent by the Human Tissue Authority.

Six samples of cartilage from different individual donors were imaged. All donors had no known diagnosis of OA, rheumatoid arthritis or other joint disease, and it has been assumed that although all the donors were in the age range of 65–86 years, the samples were all 'healthy' cartilage. Details for the donors can be found in the electronic supplementary material. Samples were procured according to the GIFT2 Research Tissue Project protocols: procurement of samples from donors was achieved within 1–7 days of death, and all donors were kept refrigerated in a standard mortuary after death. Donor knees were kept intact and frozen at −80°C before thawing immediately prior to cartilage harvesting. The samples were then immersed in phosphate-buffered solution (PBS) and imaging was started as soon as possible after harvesting (approx. 2 h).

Bovine legs were obtained from a local abattoir (John Penny and Sons, Leeds, UK) from animals which had been killed as part of the normal food chain following appropriate veterinary inspection. Cartilage was harvested from the patellofemoral groove of healthy 18-month-old cows (within 72 h of slaughter). Permission was obtained from the abattoir to use these animal tissues for research. Samples had been frozen in a standard food freezer at −20°C prior to imaging and were thus defrosted at ambient temperatures before being immersed in PBS for imaging.

Two samples are presented in the main body of the paper: one human and one bovine. Data for the five other human samples can be found in the electronic supplementary material.

2.2. Material and methods

2.2.1. MRI protocol

Imaging of the samples was achieved using a progressive saturation sequence at 9.4 T (Bruker AVANCE™ II 400 MHz). For human cartilage, a set of seven repetition times, T_R (adapted from Nissi *et al.* [26]), were used for all temperatures as given in table 1. The spin-echo time was 14 ms, slice thickness 1 mm and the in-plane resolution was 100 µm pixel^{-1}. For bovine cartilage, a set of 15 or 16 repetition times were used which were varied with temperature, as presented in table 1. The spin-echo time was 8.56 ms, slice thickness 2 mm and the in-plane resolution was 70 µm pixel^{-1} (perpendicular to the cartilage surface) by 117 µm pixel^{-1} (parallel to the surface). All signal averaging (table 1) was performed prior to image reconstruction. The number of averages and T_Rs were varied at each temperature to obtain similar signal to noise at each temperature.

For the other human samples presented in the electronic supplementary material, the number of T_Rs chosen and the matrix size were varied to account for variation in physical sample size, to ensure imaging of the sample over a range of temperatures could be obtained before significant sample degradation.

Images were obtained at a range of temperatures from 8 to 38°C. Temperature control was achieved using the water cooling system for the gradient coils on the NMR system. The samples within the imaging coils were allowed a minimum of 1 h to equilibrate with the water temperature before data collection was initiated. The temperature was monitored using a thermocouple within the bore of the magnet. Temperature data were recorded during imaging and the measurement temperature was determined as the average temperature during the imaging sequence. Fluctuations in the monitored temperature were noted to be less than 1°C at all temperatures measured.

2.2.2. T_1 and E_A profiles

T_1 relaxation time maps were calculated for each temperature measured, by fitting a mono-exponential function on a pixel-by-pixel basis (Matlab 7.14.0 R2013a, Mathworks, Inc., Natick, MA, USA), which was shown to be a good fit throughout the cartilage tissue, with $r^2 > 0.99$ in all cases. Example fits can be seen in the electronic supplementary material. T_1 relaxation time profiles were then generated through the
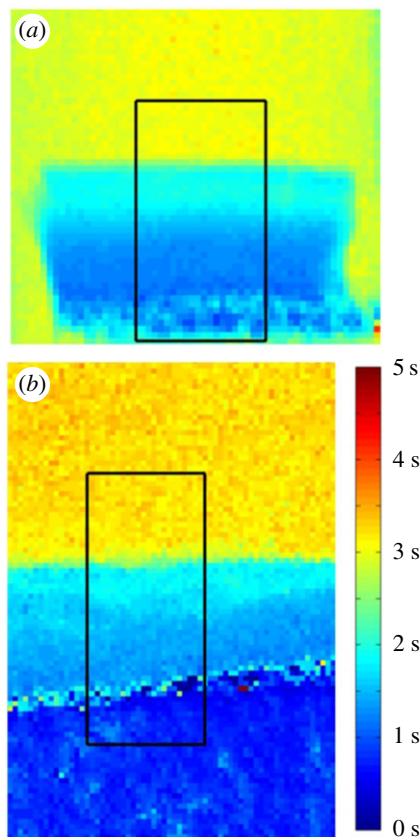
4

Figure 1. T_1 relaxation time maps of (*a*) bovine cartilage at 8°C and (*b*) human cartilage at 20°C. The rectangle in each image shows the ROI used to generate the T_1 and E_A profiles.

Table 1. Repetition times, T_R, and number of averages used in the progressive saturation sequence for the human and bovine cartilage samples at various temperatures.

sample	temperature (°C)	T_R (ms)	averages
human	9.1, 12.5, 15.9, 20.0, 25.0, 29.4, 34.5	200, 500, 1000, 1500, 2500, 4000, 8000	6
bovine	8.1	295, 458, 634, 824, 1033, 1263, 1519, 1808, 2139, 2528, 2999, 3595, 4407, 5692, 9000	4
	14.9	100, 287, 487, 703, 937, 1193, 1475, 1790, 2144, 2551, 3029, 3608, 4340, 5340, 6924, 11 040	1
	22.3	213, 440, 684, 946, 1231, 1543, 1886, 2268, 2699, 3195, 3776, 4478, 5368, 6582, 8500, 13 440	1
	30.0	100, 370, 660, 970, 1310, 1680, 2090, 2550, 3060, 3650, 4350, 5190, 6250, 7700, 10 000, 16 000	2
	38.1	622, 966, 1338, 1740, 2181, 2666, 3206, 3816, 4516, 5337, 6331, 7589, 9304, 12 017, 19 000	2

depth of the cartilage by choosing a region of interest (ROI) from the T_1 relaxation time maps, as shown in figure 1. Details of code used can be found in the electronic supplementary material.

ROIs were chosen by eye such that they included PBS from above the cartilage surface and at least some portion into the subchondral bone network below the calcified collagen, at the deepest layer of cartilage. This was done to ensure that the full thickness of cartilage was included within the ROI. The ROIs were also chosen such that there was minimal curvature of the cartilage surface.

Average T_1 relaxation time depth-wise profiles were obtained by averaging across each row (parallel to the cartilage surface) within the chosen ROI. Activation energy profiles were obtained by linearly fitting the logarithm of average T_1 relaxation times with the reciprocal of temperature, in accordance with the Arrhenius relationship [31]:

$$\frac{1}{T_1} = A \exp\left(-\frac{E_A}{RT}\right),$$

where T is the absolute temperature, R is the ideal gas constant and A is the pre-exponential factor. This linear fitting was weighted to the uncertainties determined in the fitted T_1 values. E_A was determined on a pixel-by-pixel basis and then averaged across each row using the same method as that for T_1. The surface of the cartilage was determined from the T_1 relaxation time profiles and was defined as being the midpoint of the change in T_1 relaxation time from the consistent value observed in the PBS to the smooth decrease in T_1 through the main body of cartilage. Scaling of the depth-wise profiles was achieved by using the known in-plane resolution of the images. Details of the code used can be found in the electronic supplementary material.

3. Results and discussion

3.1. T_1 relaxation time profiles

Figure 2 shows the depth-wise T_1 relaxation time profiles obtained for both bovine and human cartilage imaged in this study, for a range of temperatures. In the plots, the cartilage surface is placed at a distance of zero, with the PBS on the left (negative distance values) and the cartilage extending to the right (positive distance values). It can be seen that the T_1 of the cartilage is lower than that in the PBS and exhibits a relatively smooth decrease through the cartilage. At the deepest regions, within the calcified parts, the T_1 relaxation times become noisy due to the decreased signal intensity arising from the low water content at these depths. It can also be seen that, in the PBS and main body of the cartilage, T_1 increases with temperature.

In both cases, human and bovine, the T_1 values are seen to generally increase with increasing temperature. The rate of change of T_1 with temperature (dT_1/dT) has been determined in other studies [31]. For the cartilage in this study, this has been found to be in the range of 1.4–1.9%/°C for the human cartilage and 1.5–1.7%/°C for the bovine cartilage. These values are similar to those reported previously for other biological tissues, for example 1.4%/°C in bovine muscle [36], 1–2%/°C in liver [37] and 0.97%/°C in fat [38].

The surface of the cartilage samples was also determined using these T_1 profiles; however, as can be seen in figure 2, there is a gradient between the T_1 values in the PBS and those within the main body of the cartilage. It is believed that this is primarily due to a partial volume average artefact. Thus, the surface was defined to be the midpoint of the slope from where the T_1 values start to decrease to where the values are clearly within the main cartilage body.

The T_1 values in the region identified in figure 2 as subchondral bone are unreliable due to poor signal-to-noise ratio and the complexity of that tissue. Subchondral (cortical) bone consists of various cells embedded in a generally low-porosity matrix but which also possesses larger extracellular spaces such as the Haversian canals. In addition to the intra- and extracellular water contributions to the proton NMR signal, a component is believed to originate from protons of mobile methylene lipids [39]. The situation is potentially further complicated due to the chemical shift between the water and lipid protons, which can displace the lipid signals in the images. Also, depending on the details of the imaging sequence, chemically shifted triglyceride components from the neighbouring trabecular bone can intrude [40]. Therefore, in this region, mono-exponential T_1 fitting is no longer appropriate. However, this region is beyond the scope of investigation in this paper, which has focused on the properties of the cartilage.

Furthermore, one can see in figure 1b that the interface between the cartilage and bone is not aligned with the boundaries of the ROI. The effect of this is that the row averaging will introduce a source of error into both the cartilage and bone values in this interfacial region. Although there exist more sophisticated ways of dealing with such situations, for the simple method we employed in this work it was not possible to align both the PBS–cartilage and the cartilage–bone interfaces. Here, we chose to align the PBS–cartilage interface because it is known that the surface zone of cartilage is relatively shallow (and typically thinner than the deep zone), and this area of the cartilage is of particular importance.

T_1 plots for the other samples imaged in this study can be found in the electronic supplementary material. All samples show similar changes in T_1 with depth through the cartilage.
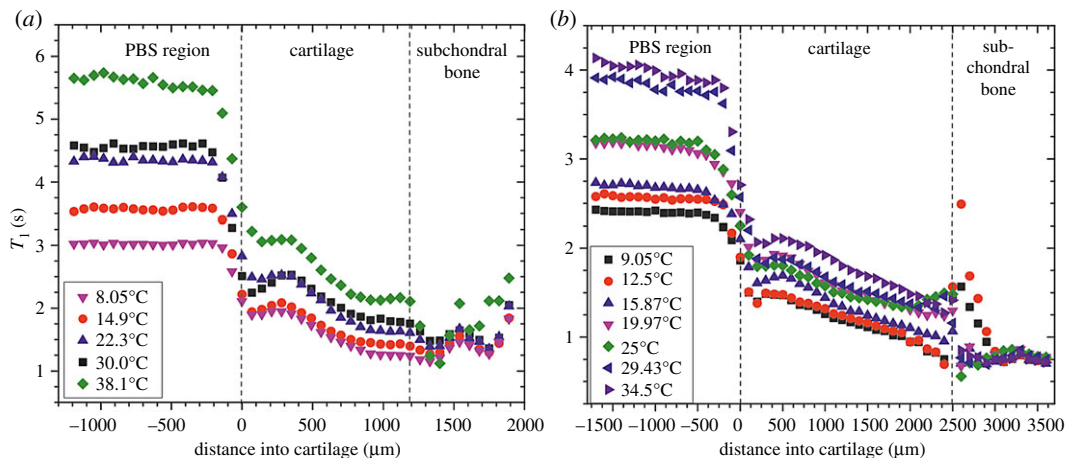
Figure 2. T_1 profiles for the selected ROI as a function of depth through the cartilage samples. (a) Bovine and (b) human. The legend in each figure panel indicates the temperature at which each T_1 profile was obtained. The lines indicating PBS, cartilage and subchondral bone are drawn to guide the eye. The PBS/cartilage dividing line is taken as the cartilage surface (0 μm), and the cartilage/bone interface is estimated as the point at which there is significant deviation from the smooth decrease in T_1. Note that error bars in T_1 are not displayed as they are smaller than the size of the data points—all errors were less than 1%.
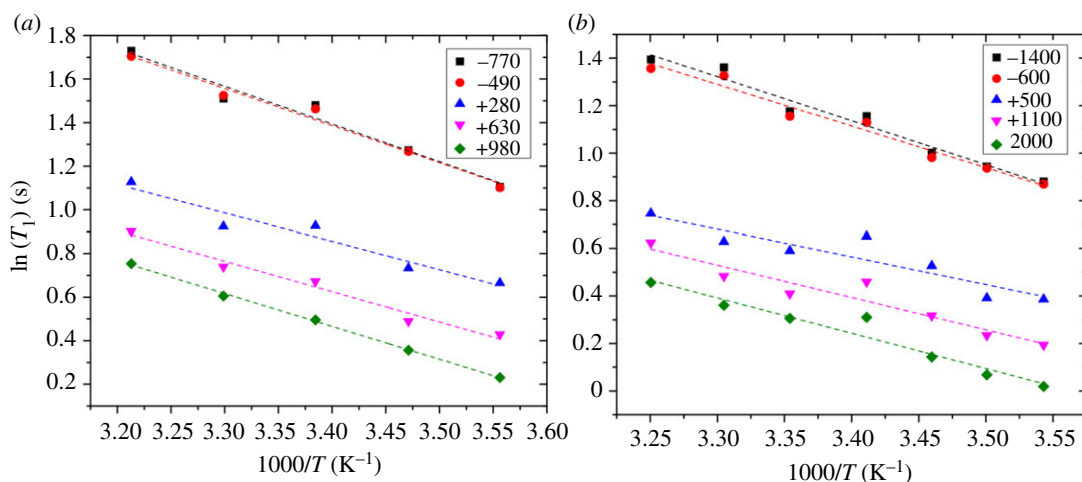

Figure 3. $\ln(T_1)$ versus $1000/T$ for (a) bovine cartilage sample and (b) human cartilage sample. The legend in each case indicates which position in the T_1 profiles (figure 2) the data were taken from. Negative numbers indicate data from above the cartilage surface (i.e. in the PBS) and positive numbers indicate data from within the cartilage tissue at different depths given in μm. Note that error bars in $\ln(T_1)$ are not displayed as they are smaller than the size of the data points.

3.2. Arrhenius plots

Figure 3 shows the Arrhenius plot for two data points selected at random in the PBS from each dataset in figure 2, and also three points from within the cartilage for each dataset, one from the upper regions, one in the middle and one towards the deeper regions of the cartilage. Figure 3 shows that the Arrhenius relationship is valid over the temperature range which has been studied, because the data show good linear dependence of $\ln(T_1)$ on $1000/T$. For all datasets visually inspected, the goodness of fit, r^2, was greater than 0.8 in all cases. The Arrhenius model therefore adequately models the data.

3.3. E_A profiles

Figure 4 shows the depth-wise E_A profiles for the ROIs selected. A different trend from that observed for the T_1 relaxation time depth-wise profiles in figure 2 is seen, which reveals that the activation energy profile is giving different and therefore additional information to that of the T_1 profile; it is this that
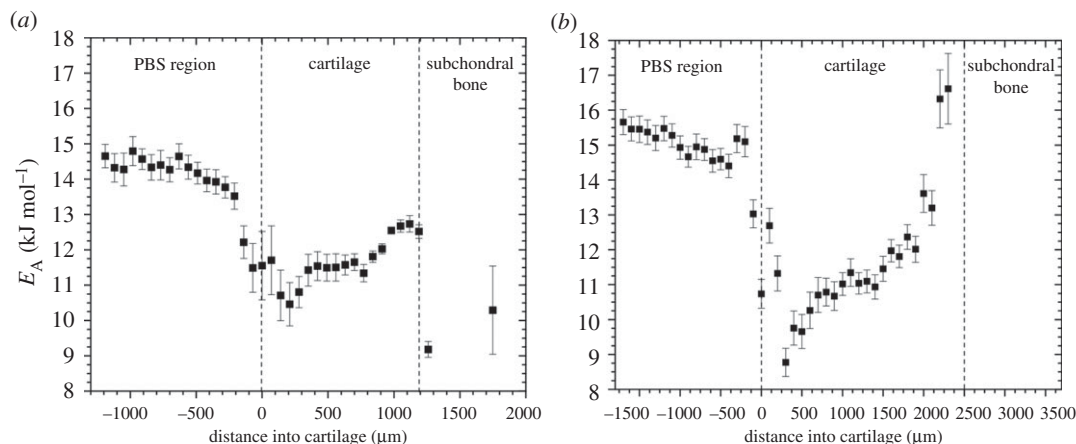
Figure 4. Activation energy profiles through the depth of the cartilage (*a*) bovine and (*b*) human. The PBS/cartilage/subchondral bone dividing lines are drawn to guide the eye and have been defined to be the same depths as those in figure 2, using the method described in that figure.

motivates this article. A detailed discussion of the nature and value of the additional information of the E_A is given in the conclusions. The E_A is lower in the cartilage than in the PBS, both in the human and bovine cartilage, and then again, in both cases, the activation energy increases in the deeper regions of the cartilage tissue. Similarly, the T_1 is lower in the cartilage than in the PBS, but in contrast to E_A, T_1 continues to decrease with increasing depth into the cartilage. There are suggestions of other features in the profile: a local minimum, close to the surface of the cartilage and also a flattening of the E_A in the middle of the cartilage. It should be noted that the initial steep decrease in the E_A seen in figure 4, from the PBS to the cartilage, could be due to the same artefact discussed in the T_1 profiles, a partial volume effect across the cartilage surface. Values within the subchondral bone are not all displayed, because the E_A values are unreliable and often negative in this region (see the paragraph above on the T_1 values and issues within the subchondral bone).

E_A profiles for other cartilage samples imaged in this study are shown in the electronic supplementary material. Similar trends can be seen in four of the other samples imaged. There will be differences in biological constituents between the samples and hence also in E_A. Additionally, an example of the fitted pre-factor from the Arrhenius model, A, for one sample is shown in the electronic supplementary material.

From data in Simpson & Carr [41], the spin–lattice E_A of pure water is $16.6 \pm 0.4 \, \text{kJ} \, \text{mol}^{-1}$, and measurement of the spin–lattice E_A of the PBS in this study (measured separately by non-imaging NMR) was $17.0 \pm 0.3 \, \text{kJ} \, \text{mol}^{-1}$, which are comparable to the values of E_A in the PBS in figure 4 of $14.7 \pm 1.0 \, \text{kJ} \, \text{mol}^{-1}$.

The interesting result to note here is that the E_A of the water within the cartilage tissue ($11 \pm 2 \, \text{kJ} \, \text{mol}^{-1}$) is actually lower than that of the PBS ($14.7 \pm 1.0 \, \text{kJ} \, \text{mol}^{-1}$) or pure water ($16.6 \pm 0.4 \, \text{kJ} \, \text{mol}^{-1}$). We suggest that this is because the rotational dynamics of water is disrupted by the confinement of the water within the cartilage matrix. This is similar to how the confinement of water within pores lowers the melting and freezing point of water [42,43]. It has also been found for other systems that the diffusion activation energies of liquids are reduced by confinement into pores or channels, showing that the translational dynamics are affected by confinement [44]. Indeed, the lowering of the E_A in biological tissues below the value of pure water has previously been reported for relaxation times in muscle tissue [33] and diffusion in white matter [32]. Molecular dynamic simulations show that the confinement of water has a notable effect on the hydrogen bond network of water extending up to approximately 0.1 µm from a confining surface [45]. Neutron diffraction experiments have shown that confined water phases are radically different from free (unconfined) phases owing to the presence of cross-interactions between water and surface substrate, and that the perturbation induced by the wall extends throughout the confined region [46].

Diffusion, involving translational motion, will (in general) have a higher activation energy than one found from T_1 or for rotational motion. According to the work of O'Reilly [47], the diffusion activation energy is the sum of rotational activation energy plus the work required to create a 'vacancy' for the diffusing molecule to move into. Our argument is that a lowering in diffusion activation energy caused

by confinement, as reported in the literature, supports our explanation of a lowered activation energy for T_1 in cartilage due to confinement. The fact that the absolute values will be different between the two different mechanisms does not detract from the point that the values are decreased by confinement.

We now suggest that the subsequent increase in E_A with depth is related to the association of the water to the other macromolecular constituents in the cartilage tissue, because it is well known that collagen density [4,48] and GAG density [4] increase with depth, while water density decreases [49]. There are, to a first approximation, effectively two types of water within cartilage tissue, relatively mobile 'bulk' water and relatively immobile 'bound' water that is associated with or bound to the macromolecules within the tissue. The bulk water has a reduced E_A because of confinement within the tissue pores as suggested above, and the bound water actually has a higher E_A because it is directly associated with or bound to macromolecules within the tissue. This additional binding increases the activation energy required for rotation, which subsequently increases the activation energy for spin–lattice relaxation. It should be noted that water that is confined within pores is not necessarily directly interacting with the confining surface, and hence is not necessarily part of the bound water in the sense described above. The T_1 measurement, and thus the E_A value, is approximately a weighted average of these two types of water, and because the bulk water constitutes a greater fraction closer to the articular surface [49], the net effect is that E_A is lower than that of pure water near the surface. Deeper in the cartilage, this weighted average changes in favour of the bound water, because a greater fraction of the water is now directly associated with the macromolecules in this less water dense environment, and the measured E_A increases because of this.

4. Conclusion

Human and bovine cartilages were examined using MRI to measure the T_1 in the tissue samples as a function of depth. This was repeated for a range of temperatures in order to determine the spin–lattice relaxation activation energy as a function of depth through the cartilage, using an Arrhenius model. Depth-wise T_1 profiles through the cartilage matched values reported previously and showed similar trends through the depth of the tissues at all temperatures [26]. It was shown that the T_1 relaxation time as a function of temperature, within the cartilage samples, follows Arrhenius-type behaviour. From this, an activation energy for the NMR relaxation process was determined. The activation energy within the cartilage ($11 \pm 2 \, \text{kJ mol}^{-1}$) is lower than that of pure water ($16.6 \pm 0.4 \, \text{kJ mol}^{-1}$) and PBS ($14.7 \pm 1.0 \, \text{kJ mol}^{-1}$). Profiles of the depth-wise activation energy were shown in figure 4, which show a different behaviour from those of the T_1 relaxation time profiles, as shown in figure 3. The activation energy increases with depth, but is generally lower than that of pure water. This is to be compared with the T_1 relaxation time which decreases with depth and is lower than that of pure water. This difference in behaviour indicates that the activation energy is giving additional information about the cartilage system.

It is important to note that the activation energy contains new and additional information to the spin–lattice relaxation time, T_1. Though the Arrhenius equation links the spin–lattice relaxation time directly to the activation energy, it is not known *a priori*; without varying the temperature, it is not possible to determine the value of E_A. It is the energy barrier that has to be overcome for T_1 relaxation to occur. The T_1 relaxation time at high fields (greater than 100 MHz) is determined predominantly by the rotational motion of, in this case, water molecules. Therefore, the NMR-determined E_A is effectively a measure of the rotational E_A of the water molecules. These water molecules exist in a variety of states, such as 'free' and 'bound' [30], but in our work only one spin–lattice relaxation time is evident. Hence, the E_A is a weighted average of the different environments and includes the effect of confinement on the arrangement of water through its effect on inter-water molecule interactions. This makes the E_A potentially interesting, as it is a measure of confinement and the interactions of the water molecules with other constituents within cartilage. Changes in composition of the cartilage, through ageing or damage, are therefore expected to alter the activation energy and hence it might prove to be a useful tool for cartilage (*in vitro*) research. As shown in figures 2 and 4, the dependence of the E_A on depth is different from that of the T_1 relaxation time, confirming our hypothesis that the E_A reveals additional information to that of the T_1 relaxation time.

Although further work is required to understand the physical meaning of E_A, we suggest that the decrease in the activation energy, when compared with that for pure water, is due to the confinement of the water within the cartilage matrix, including by action of pores. Furthermore, we suggest that the subsequent increase of E_A with depth is due to the increase in association and bonding of the water with

the other constituents deeper within the cartilage. This is because with increasing depth the water density itself decreases, while the density of other components increases [4], giving rise to more interactions between the water and those components. The increase of these interactions between the water and its surroundings leads to an increase in the activation energy for rotational motion of the water. If our hypothesis is correct, then this could make the activation energy a useful measure of the amount of bulk and bound water, and hence could be a novel way to detect structural changes, for instance those associated with OA, in cartilage (*in vitro*).

References

1. Binks DA, Hodgson RJ, Ries ME, Foster RJ, Smye W, McGonagle D, Radjenovic A. 2013 Quantitative parametric MRI of articular cartilage: a review of progress and open challenges. *Br. J. Radiol.* **86**, 20120163. (doi:10.1259/bjr.20120163)

2. Mow VC, Huiskes R. 2005 *Basic orthopaedic biomechanics and mechano-biology*, 3rd edn. Philadelphia, PA: Lippincott Williams and Wilkins.

3. Vaca-González JJ, Guevara JM, Moncayo MA, Castro-Abril H, Hata Y, Garzón-Alvarado DA. 2017 Biophysical stimuli: a review of electrical and mechanical stimulation in hyaline cartilage. *Cartilage* (online). (doi:10.1177/1947603517730637)

4. Wilson W, van Donkelaar CC, van Rietbergen R, Huiskes R. 2005 The role of computational models in the search for the mechanical behavior and damage mechanisms of articular cartilage. *Med. Eng. Phys.* **27**, 810–826. (doi:10.1016/j.medengphy.2005.03.004)

5. Pacifici M. 2014 Introduction to the mini-review series 'Articular cartilage: biology, pathology and repair'. *Matrix. Biol.* **39**, 1. (doi:10.1016/j.matbio.2014.08.004)

6. McGonagle D, Tan AL, Carey J, Benjamin M. 2010 The anatomical basis for a novel classification of osteoarthritis and allied disorders. *J. Anat.* **216**, 279–291. (doi:10.1111/j.1469-7580.2009.01186.x)

7. Baldassarri M, Goodwin JSL, Farley ML, Bierbaum BE, Goldring SR, Goldring MB, Burstein D, Gray ML. 2007 Relationship between cartilage stiffness and dGEMRIC index: correlation and prediction. *J. Orthop. Res.* **25**, 904–912. (doi:10.1002/jor.20378)

8. Nieminen MT, Rieppo J, Toyras J, Hakumaki JM, Silvennoinen J, Hyttinen MM, Helminen HJ, Jurvelin JS. 2001 T-2 relaxation reveals spatial collagen architecture in articular cartilage: a comparative quantitative MRI and polarized light microscopic study. *Magn. Reson. Med.* **46**, 487–493. (doi:10.1002/mrm.1218)

9. Nissi MJ, Rieppo J, Toyras J, Laasanen MS, Kiviranta I, Jurvelin JS, Nieminen MT. 2006 T-2 relaxation time mapping reveals age- and species-related diversity of collagen network architecture in articular cartilage. *Osteoarthr. Cartil.* **14**, 1265–1271. (doi:10.1016/j.joca.2006.06.002)

10. Xia Y, Moody JB, Alhadlaq H. 2002 Orientational dependence of T_2 relaxation in articular cartilage: a microscopic MRI (µMRI) study. *Magn. Reson. Med.* **48**, 460–469. (doi:10.1002/mrm.10216)

11. Bashir A, Gray ML, Hartke J, Burstein D. 1999 Nondestructive imaging of human cartilage glycosaminoglycan concentration by MRI. *Magn. Reson. Med.* **41**, 857–865. (doi:10.1002/(SICI)1522-2594(199905)41:5<857::AID-MRM1>3.0.CO;2-E)

12. Dunn TC, Lu Y, Jin H, Ries MD, Majumdar S. 2004 T2 relaxation time of cartilage at MR imaging: comparison with severity of knee osteoarthritis. *Radiology* **232**, 592–598. (doi:10.1148/radiol.2322030976)

13. Eckstein F, Burstein D, Link TM. 2006 Quantitative MRI of cartilage and bone: degenerative changes in osteoarthritis. *NMR Biomed.* **19**, 822–854. (doi:10.1002/nbm.1063)

14. Zarins ZA, Bolbos RI, Pialat JB, Link TM, Li X, Souza RB, Majumdar S. 2010 Cartilage and meniscus assessment using T1rho and T2 measurements in healthy subjects and patients with osteoarthritis. *Osteoarthr. Cartil.* **18**, 1408–1416. (doi:10.1016/j.joca.2010.07.012)

15. Fragonas E, Mlynárik V, Jellús V, Micali F, Piras A, Toffanin R, Rizzo R, Vittur F. 1998 Correlation between biochemical composition and magnetic resonance appearance of articular cartilage. *Osteoarthr. Cartil.* **6**, 24–32. (doi:10.1053/joca.1997.0089)

16. Xia Y, Moody JB, Burton-Wurster N, Lust G. 2001 Quantitative in situ correlation between microscopic MRI and polarized light microscopy studies of articular cartilage. *Osteoarthr. Cartil.* **9**, 393–406. (doi:10.1053/joca.2000.0405)

17. Rautiainen J et al. 2015 Multiparametric MRI assessment of human articular cartilage degeneration: correlation with quantitative histology and mechanical properties. *Magn. Reson. Med.* **74**, 249–259. (doi:10.1002/mrm.25401)

18. Lüssea S, Claassen H, Gehrke T, Hassenpflug J, Schünke M, Heller M, GlüEr C-C. 2000 Evaluation of water content by spatially resolved transverse relaxation times of human articular cartilage. *Magn. Reson. Imaging* **18**, 423–430. (doi:10.1016/S0730-725X(99)00144-7)

19. Akella SVS, Regatte RR, Gougoutas AJ, Borthakur A, Shapiro EM, Kneeland JB, Leigh JS, Reddy R. 2001 Proteoglycan-induced changes in $T_{1\rho}$-relaxation of articular cartilage at 4 T. *Magn. Reson. Med.* **46**, 419–423. (doi:10.1002/mrm.1208)

20. Wheaton AJ, Dodge GR, Elliott DM, Nicoll SB, Reddy R. 2005 Quantification of cartilage biomechanical and biochemical properties via $T_{1\rho}$ magnetic resonance imaging. *Magn. Reson. Med.* **54**, 1087–1093. (doi:10.1002/mrm.20678)

21. Borthakur A, Mellon E, Niyogi S, Witschey W, Kneeland JB, Reddy R. 2006 Sodium and $T_{1\rho}$ MRI for molecular and diagnostic imaging of articular cartilage. *NMR Biomed.* **19**, 781–821. (doi:10.1002/nbm.1102)

22. Reddy R, Insko EK, Noyszewski EA, Dandora R, Kneeland JB, Leigh JS. 1998 Sodium MRI of human articular cartilage *in vivo*. *Magn. Reson. Med.* **39**, 697–701. (doi:10.1002/mrm.1910390505)

23. Shapiro EM, Borthakur A, Gougoutas A, Reddy R. 2002 ^{23}Na MRI accurately measures fixed charge density in articular cartilage. *Magn. Reson. Med.* **47**, 284–291. (doi:10.1002/mrm.10054)

24. Lin PC, Reiter DA, Spencer RG. 2009 Sensitivity and specificity of univariate MRI analysis of experimentally degraded cartilage. *Magn. Reson. Med.* **62**, 1311–1318. (doi:10.1002/mrm.22110)

25. Ward KM, Aletras AH, Balaban RS. 2000 A new class of contrast agents for MRI based on proton chemical exchange dependent saturation transfer (CEST). *J. Magn. Reson.* **143**, 79–87. (doi:10.1006/jmre.1999.1956)

26. Nissi MJ, Rieppo J, Töyräs J, Laasanen MS, Kiviranta I, Nieminen MT, Jurvelin JS. 2007 Estimation of mechanical properties of articular cartilage with MRI – dGEMRIC, T_2 and T_1 imaging in different species with variable stages of maturation. *Osteoarthr. Cartil.* **15**, 1141–1148. (doi:10.1016/j.joca.2007.03.018)

27. Berberat JE, Nissi MJ, Jurvelin JS, Nieminen MT. 2009 Assessment of interstitial water content of articular cartilage with T_1 relaxation. *Magn. Reson. Imaging* **27**, 727–732. (doi:10.1016/j.mri.2008.09.005)

28. Burstein D, Velyvis J, Scott KT, Stock KW, Kim YJ, Jaramillo D, Boutin RD, Gray ML. 2001 Protocol issues for delayed Gd(DTPA)-enhanced MRI: (dGEMRIC) for clinical evaluation of articular cartilage. *Magn. Reson. Med.* **45**, 36–41. (doi:10.1002/1522-2594(200101)45:1<36::AID-MRM1006>3.0.CO;2-W)

29. Tiderius CJ, Olsson LE, Leander P, Ekberg O, Dahlberg L. 2003 Delayed gadolinium-enhanced MRI of cartilage (dGEMRIC) in early knee osteoarthritis. *Magn. Reson. Med.* **49**, 488–492. (doi:10.1002/mrm.10389)

30. Damion RA, Pawaskar SS, Ries ME, Ingham E, Williams S, Jin Z, Radjenovic A. 2012 Spin–lattice relaxation rates and water content of freeze-dried articular cartilage. *Osteoarthr. Cartil.* **20**, 184–190. (doi:10.1016/j.joca.2011.12.005)

31. Rieke V, Butts Pauly K, Pauly KB. 2008 MR thermometry. *J. Magn. Reson. Imaging* **27**, 376–390. (doi:10.1002/jmri.21265)

32. Dhital B, Labadie C, Möller HE, Turner R. 2011 Activation energies for water diffusion in ex-vivo white matter vol. 19. In *Proceedings of the International Society for Magnetic Resonance in Medicine, Montreal, Canada, 6–13 May*, p. 78. ISMRM. See https://www.ismrm.org/11/Session08.htm.

33. Fung BM, McGaughy TW. 1979 Study of spin-lattice and spin-spin relaxation-times of 1H, 2H, and 17O in muscle water. *Biophys. J.* **28**, 293–303. (doi:10.1016/S0006-3495(79)85177-2)

34. Quesson B, de Zwart JA, Moonen CTW. 2000 Magnetic resonance temperature imaging for guidance of thermotherapy. *J. Magn. Reson. Imaging* **12**, 525–533. (doi:10.1002/1522-2586(200010)12:4<525::AID-JMRI3>3.0.CO;2-V)

35. Wright A. 2014 *Leeds tissue bank: making a GIFT for research Vol. 2014*. Leeds, UK: University of Leeds.

36. Cline HE, Hynynen K, Hardy CJ, Watkins RD, Schenck JF, Jolesz FA. 1994 MR temperature mapping of focused ultrasound surgery. *Magn. Reson. Med.* **31**, 628–636. (doi:10.1002/mrm.1910310608)

37. Matsumoto R, Oshio K, Jolesz FA. 1992 Monitoring of laser and freezinginduced ablation in the liver with T1-weighted MR imaging. *J. Magn. Reson. Imaging* **2**, 555–562. (doi:10.1002/jmri.1880020513)

38. Hynynen K, McDannold N, Mulkern RV, Jolesz FA. 2000 Temperature monitoring in fat with MRI. *Magn. Reson. Med.* **43**, 901–904. (doi:10.1002/1522-2594(200006)43:6<901::AID-MRM18>3.0.CO;2-A)

39. Horch RA, Nyman JS, Gochberg DF, Dortch RD, Does MD. 2010 Characterization of ^{1}H NMR signal in human cortical bone for magnetic resonance imaging. *Magn. Reson. Med.* **64**, 680–687. (doi:10.1002/mrm.22459)

40. Karampinos DC, Melkus G, Baum T, Bauer JS, Rummeny EJ, Krug R. 2014 Bone marrow fat quantification in the presence of trabecular bone: initial comparison between water-fat imaging and single-voxel MRS. *Magn. Reson. Med.* **71**, 1158–1165. (doi:10.1002/mrm.24775)

41. Simpson JH, Carr HY. 1958 Diffusion and nuclear spin relaxation in water. *Phys. Rev.* **111**, 1201. (doi:10.1103/PhysRev.111.1201)

42. Babushkina TA, Klimova TP, Shtykova AV, Dembo KA, Volkov VV, Khripunov AK, Klechkovskaya VV. 2010 Study of the gel films of *Acetobacter xylinum* cellulose and its modified samples by ^{1}H NMR cryoporometry and small-angle X-ray scattering. *Crystallogr. Rep.* **55**, 312–317. (doi:10.1134/S1063774510020252)

43. Hay JN, Laity PR. 2000 Observations of water migration during thermoporometry studies of cellulose films. *Polymer* **41**, 6171–6180. (doi:10.1016/S0032-3861(99)00828-9)

44. Lingwood MD, Zhang ZY, Kidd BE, McCreary KB, Hou JB, Madsen LA. 2013 Unraveling the local energetics of transport in a polymer ion conductor. *Chem. Commun.* **49**, 4283–4285. (doi:10.1039/c2cc37173a)

45. Fan Y, Gao YQ. 2010 Long-range effects of confinement on water structure. *J. Phys. Chem. B* **114**, 4246–4251. (doi:10.1021/jp9086392)

46. Mancinelli R. 2010 The effect of confinement on water structure. *J. Phys. Condens. Matter* **22**, 404213. (doi:10.1088/0953-8984/22/40/404213)

47. O'Reilly DE. 1968 Self-diffusion coefficients and rotational correlation times in polar liquids. *J. Chem. Phys.* **49**, 5416–5420. (doi:10.1063/1.1670066)

48. Kokkonen HT *et al.* 2011 Computed tomography detects changes in contrast agent diffusion after collagen cross-linking typical to natural aging of articular cartilage. *Osteoarthr. Cartil.* **19**, 1190–1198. (doi:10.1016/j.joca.2011.07.008)

49. Wilson W, Huyghe JM, van Donkelaar CC. 2007 Depth-dependent compressive equilibrium properties of articular cartilage explained by its composition. *Biomech. Model. Mechanobiol.* **6**, 43–53. (doi:10.1007/s10237-006-0044-z)